J Mater Sci (2007) 42:9877–9887
DOI 10.1007/s10853-007-1685-8

Extreme value analysis of ductile fracture surface by dimpled rupture associated with fracture behavior of tensile specimens

M. Ohashi

Received: 24 May 2006 / Accepted: 12 March 2007 / Published online: 20 August 2007

Abstract The extreme value analysis of the ductile fracture surface by dimpled rupture was performed associated with the fracture behavior of spheroidal graphite cast iron. A wide variation in the sizes of dimples is commonly observed on the ductile fracture surfaces of most materials. A statistical approach should be included to quantify the ductile fracture surfaces and relate them to the fracture behavior of the materials. The distributions of both the maximum dimple sizes in the unit area and the lateral growth factors of maximum dimples were well expressed as largest extreme value distributions for the tensile specimens with various plastic constraint factors. The location parameter, that is, the mode or highest point of the distribution, was directly related to the fracture strain and stress of the tensile specimen. Thus, the fracture behavior of the tensile specimens could be estimated approximately once the location parameter of the distribution is known by fractographic examination. Hence, extreme value analysis could be used as an attractive method for quantitative description of the ductile fracture surfaces correlated with the fracture behavior of spheroidal graphite cast iron.

Introduction

Ductile fracture is a common failure mode in a large percentage of engineering components, which occurs due to initiation, subsequent growth, and coalescence of voids nucleating around second phase particles. Various models have been developed to describe the ductile fracture process under triaxial stress fields by the growth of voids [1, 2]. The solutions show that a highly developed triaxial stress state enhances the growth of voids and reduces the fracture strain by promoting the coalescence of voids. The triaxial stress state with superposition of hydrostatic stresses has a great influence on the ductile fracture process.

On the other hand, examination of the fracture surfaces with a scanning electron microscope is a standard practice to determine the cause of failure. However, fractographic examination provides little quantitative information regarding the fracture behavior of the materials. A quantitative description of the fracture surfaces has been attracting much interest because the fracture surfaces contain a wealth of information. Therefore, a variety of studies have been performed to quantitatively describe the ductile fracture surfaces.

For instance, the average spacing of dimples on the ductile fracture surfaces was examined to correlate them with the average inclusion distance [3]. The inclusion spacing is closely related to the ductility of the material. The extent of primary void growth, which was defined as the size ratio of voids to the second phase particles nucleating the voids was also investigated as a measure of the toughness of high strength materials [4–6]. In addition, the small-scale roughness of the microvoid fracture surface determined by the ratio of dimple depth to width was discussed as a measure of the local fracture strain and toughness of the material [7, 8]. Moreover, the energy required to form a ductile fracture surface was estimated from the measurements of dimple size, and was used to compute the fracture toughness of the material [9]. Furthermore, the dimple size on the ductile fracture surface was correlated with changes in void growth rate by triaxial

M. Ohashi (✉)
National Research Institute of Police Science,
6-3-1,Kashiwanoha, Kashiwa, Chiba 277-0882, Japan
e-mail: ohashi@nrips.go.jp

stress state [10] and void nucleation density by hydrogen [8, 11]. The dimple size could be either increased or decreased by an accelerated void growth rate by triaxial stress state [10] or an increased void nucleation density by hydrogen [8, 11].

However, the changes in dimple size [3, 10], extent of primary void growth [4–6], micro-roughness [7], and dimple size ratio [8, 11] on the ductile fracture surface were typically reported as mean values. On the other hand, a wide variation in the sizes of dimples was commonly observed on the ductile fracture surfaces. This is because most materials contain second phase particles, which are randomly distributed in the materials. The second phase particles act as dominant nuclei for dimples during deformation. Thus, the random variation in the sizes of dimples is an intrinsic nature of the ductile fracture surfaces. The dimple sizes must be analyzed from a statistical point of view for a quantitative fractographic study.

A study on the statistical variation of the sizes of dimples has been neglected so far, and very little is known about the statistical nature of dimple size distribution. The statistical approach should be included to quantify the ductile fracture surfaces and relate them to the fracture behavior of the materials. Thus, extreme value analyses of the ductile fracture surfaces were performed as a particular application of the statistical approach associated with the fracture behavior of spheroidal graphite cast iron. The statistical theory of extreme values [12] has been applied to estimate the maximum pit depth in corrosion research [13–16], the maximum fatigue crack length for life prediction of mechanical components [17], and the largest defect size in the stressed material for predicting the lower bounds of fatigue strength [18, 19]. It was used to explain the statistical variation in dimple sizes and quantitatively describe the ductile fracture surfaces.

The fracture surfaces of spheroidal graphite cast iron with ferritic matrix were almost completely covered by dimples under static tensile loading. The maximum dimple in a given field of view is the one that nucleates first from the large graphite and grows under the influence of varying degrees of triaxial stress state. It is expected to provide useful information as to the magnitude of stress triaxiality developed in the specimen. In addition, the lateral growth factor of the maximum dimple is also expected to provide valuable information about the intensity of the triaxial stress state. The lateral growth factor is the size ratio of the maximum dimple to the graphite nucleating the dimple. It can be measured conveniently from ductile fracture surfaces. Thus, extreme value analyses of both the maximum dimple sizes and lateral growth factors of maximum dimples were performed to quantify the ductile fracture surfaces and relate them to the fracture behavior of the tensile specimens with various stress triaxialities.

Experimental procedure

Material and tensile specimens

The material tested was a spheroidal graphite cast iron with ferritic matrix. Its chemical composition and mechanical properties are given in Table 1. The yield stress was defined as a stress level related to the onset of 0.2% plastic strain. The material received in as-cast condition was annealed at 900 °C for 3 h. The microstructure of the material is illustrated in Fig. 1.

The geometry and dimensions of the tensile specimens are presented in Fig. 2. Both unnotched and notched tensile specimens with different notch root radii of 6, 3, and 1 mm were used to obtain a wide range of stress triaxialities. This is a particularly convenient geometry since various stress triaxialities can be obtained by simply alternating the notch acuity [20–22]. Notch acuity was chosen to ensure ductile fracture initiation in the center of the tensile specimen [10]. The notched specimens with three notch acuities are described as R6, R3, and R1 mm notched specimens, respectively. All specimens were loaded up to failure under tensile loading. Tensile tests were conducted at room temperature at a crosshead speed of 1 mm/min.

Plastic constraint factor

As a measure to express the degree of stress triaxiality, the plastic constraint factor was determined for each notched specimen. A triaxial stress system developed in the notched specimen constrains the lateral contraction of the material in the minimum section. The lateral constraint raises the axial stress to initiate the plastic deformation. Thus, the nominal stress on the minimum section at which the stress–displacement curve deviates initially from linearity was defined as the general yield stress. Then, the plastic constraint factor was determined as the ratio of the general yield stress to the yield stress to characterize the magnitude of triaxial stresses.

The physical significance of plastic constraint was used to explain the notch brittleness of the materials [23]. As the notch acuity, notch depth, and plate thickness are increased, a triaxial stress state is developed sharply. Consequently, the plastic constraint increases and the material fails with a lower amount of plastic deformation.

Table 1 Chemical composition (wt.%) and mechanical properties of the material

C	Si	Mn	P	S	Mg
3.7	2.7	0.26	0.059	0.017	0.086
Yield stress (MPa)		Tensile strength (MPa)		Elongation (%)	
298.8		424.1		21.7	

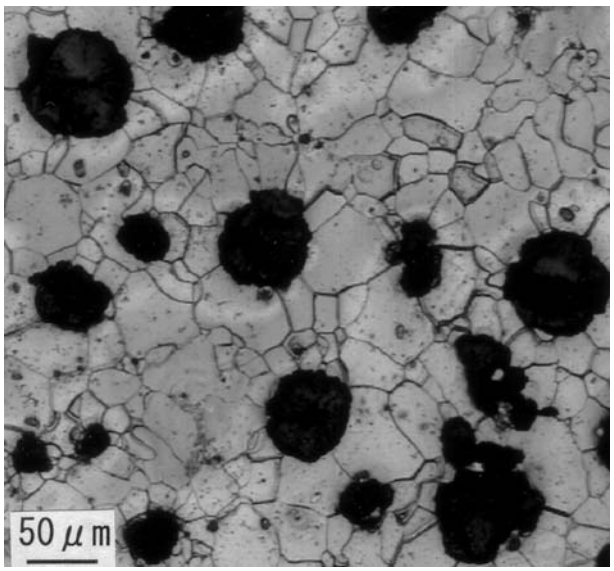

Fig. 1 Microstructure of the material

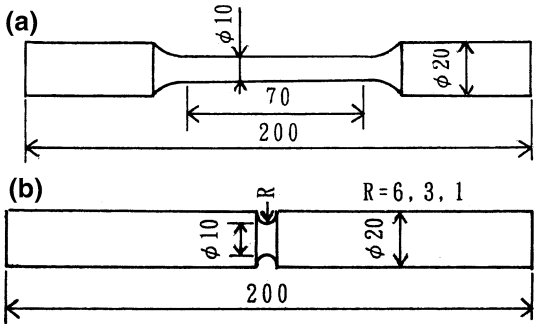

Fig. 2 Geometry and dimensions of tensile specimens (dimensions in mm) (**a**) Unnotched tensile specimen (**b**) Notched tensile specimen

An elastic-plastic stress analysis for a notched bar was performed to explain the temperature dependence of the fracture toughness based on a critical tensile stress criterion [24]. A similar ratio of maximum stress to yield stress has occasionally been used to express the local stress intensification [24, 25]. It is generally recognized that brittle fracture occurs due to a cleavage mechanism when the maximum local stress exceeds the critical tensile stress, which is relatively independent of temperature [25–28].

In this study, the plastic constraint factor was obtained from a simple graphical procedure instead of an elastic-plastic computed stress analysis. However, it could be used as a good measure to express the intensity of the triaxial stress field developed in the notched specimen.

Fracture strains and stresses of tensile specimens

The fracture strain of the tensile specimen was determined from the reduction in net area as

$$\varepsilon_p = 2\ln(d_0/d) \quad (1)$$

where ε_p is the fracture strain, d_0 is the initial value of the diameter, and d is the final value of the diameter of the minimum section. The diameters d_0 and d were measured with a profile projector before and after the tensile test. The fracture stress was defined as the average stress at fracture at the final cross-sectional area.

Fractographic examination

Fractographic examination was performed with a scanning electron microscope to clarify the fracture mechanism and determine the distribution of the maximum dimple sizes on the fracture surfaces. All fracture surfaces taken from the broken tensile specimens were aligned normal to the electron beam in the scanning electron microscope during the measurement of dimple sizes. A magnification of 300 times was selected on the basis of dimple sizes on the fracture surfaces. The scanning electron fractography proved that almost all fracture surfaces were covered with dimples of various sizes. However, a slight amount of cleavage was observed in the central portion of the fracture surfaces of R1 mm notched specimens. The area fraction covered by dimples was then measured for 20 views at an interval of 2 mm on the fracture surfaces. The area of each view was 0.13 mm^2.

Next, extreme value analysis of the ductile fracture surfaces was performed within a square area of 9 mm^2 in the central region of the ductile fracture surfaces. A ductile fracture due to microvoid coalescence initiates in the center of the tensile specimens with mild notch or local necking [10, 20–22, 29], where stress triaxiality is most severe. The square area examined was divided into 70 unit areas. The size of the unit area was 0.13 mm^2. First, the maximum dimple sizes in each unit area were measured to generate the maximum dimple size distribution. Second, the sizes of the graphites nucleating the maximum dimples were measured to obtain the distribution of the lateral growth factors of the maximum dimples. The lateral growth factor is essentially identical to the extent of primary void growth [4–6]. The sizes of the maximum dimples and graphites were readily measured on the scanning electron micrographs as the average of the maximum and minimum apparent diameters.

In addition, the sizes of the graphites within the square area of 9 mm^2 in the central portion of the fracture surfaces were measured to obtain their size distribution. The true diameters of graphites could be easily obtained from the fracture surfaces. All graphites with a diameter greater than 10 μm were measured on the fracture surfaces of three R1 mm notched specimens.

Results and discussion

Nominal stress–displacement curves of tensile specimens

Figure 3 shows typical plots of the nominal stress–displacement curves of unnotched and notched specimens with three notch acuities. The nominal stress on the minimum section is plotted against crosshead displacement until final fracture. In the conventional unnotched specimen, the nominal stress rises as the material strain-hardens after the initial elastic response and reaches a maximum value with increasing plastic deformation. Then, the stress starts to fall off slightly and further loading leads to final failure in a ductile mode.

In contrast, the nominal stress–displacement curves of notched specimens exhibit a different response of almost elastic behavior. Figures 4–6 show the detailed stress–displacement responses of R6 mm, R3 mm, and R1 mm notched specimens, respectively. The flow curves of notched specimens are not perfectly elastic but exhibit a different degree of non-linear behavior before failure. The general yield stress of the notched specimen, which was determined as the beginning of plastic behavior is marked as σ_{GY} in Figs. 4–6.

In Fig. 4, the stress–displacement curve of the R6 mm notched specimen continues to rise to a fracture stress with a certain amount of non-linear behavior, while, the flow curve of the R3 mm notched specimen shows a lower amount of non-linearity in Fig. 5. The R1 mm notched specimen fails almost simultaneously with general yield, and exhibits just minor non-linearity in Fig. 6. The different response of elastic-plastic behavior for each notched specimen could be explained by the development of stress triaxiality with increasing notch acuity. The magnitude of the triaxial stress field increases as the notch acuity is increased. As a result, the R1 mm notched specimens exhibit high general yield stresses of about 510–530 MPa, and fail with a small amount of plastic deformation.

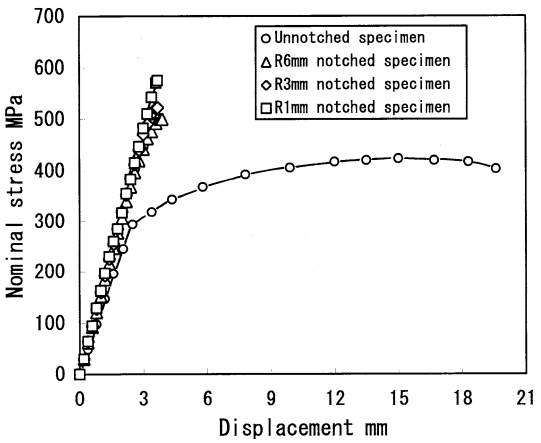

Fig. 3 Nominal stress–displacement curves of unnotched and notched tensile specimens

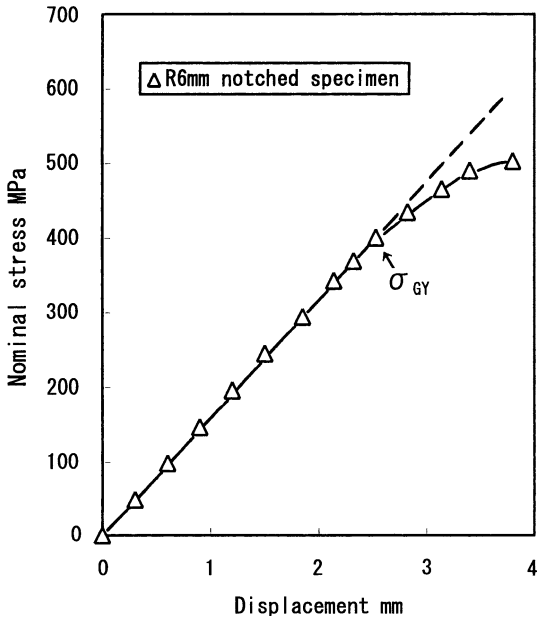

Fig. 4 Nominal stress–displacement curve of R6 mm notched specimen

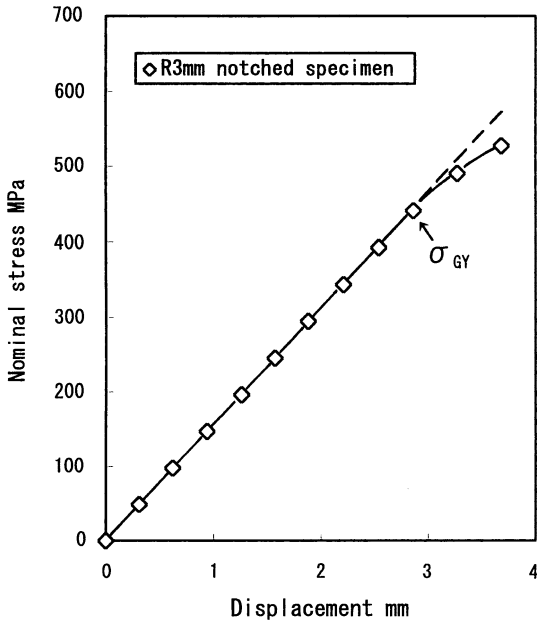

Fig. 5 Nominal stress–displacement curve of R3 mm notched specimen

Variation of fracture stress and strain with plastic constraint factor

From a series of measurements of stress–displacement curves, the plastic constraint factor was determined as the

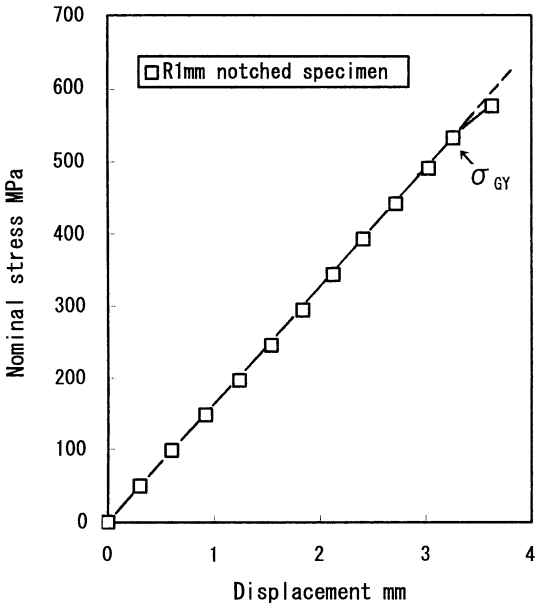

Fig. 6 Nominal stress–displacement curve of R1 mm notched specimen

ratio of the general yield stress to the yield stress for each notched specimen. It was taken to be 1 for the unnotched specimens as a necessity, and increased to about 1.7–1.8 for the R1 mm notched specimens.

Figure 7 illustrates the variation of fracture stress with plastic constraint factor. The fracture stress increased to a greater value with increasing plastic constraint factor. On the other hand, Fig. 8 shows the variation of fracture strain with plastic constraint factor. The fracture strain decreased sharply with increasing plastic constraint factor. Both the fracture stress and strain, which characterize the fracture behavior of the tensile specimen varied consistently with increasing plastic constraint factor. As a consequence, the

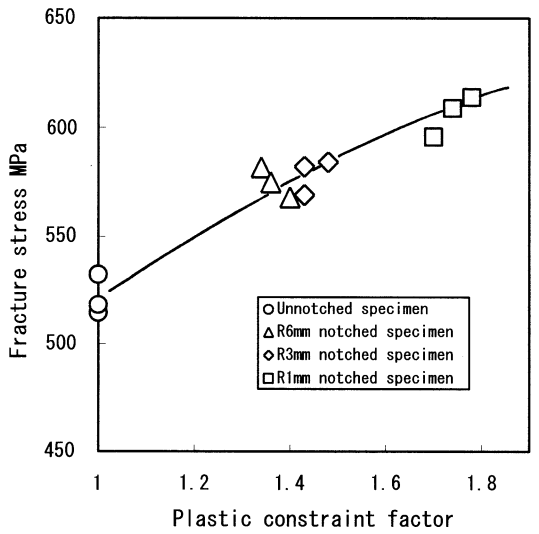

Fig. 7 Variation of fracture stress with plastic constraint factor

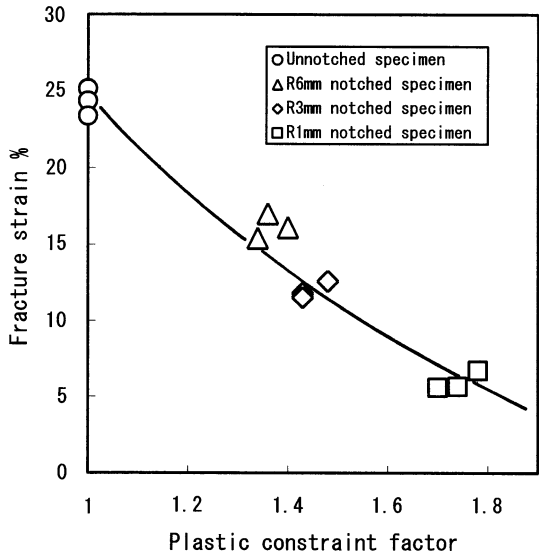

Fig. 8 Variation of fracture strain with plastic constraint factor

plastic constraint factor could be used as a good measure to express the magnitude of the triaxial stress field developed in the notched specimen.

Correlation between dimple area fraction and fracture strain

Figure 9 demonstrates the typical appearance of the macroscopic fracture surfaces of the unnotched and notched specimens. The macroscopic appearance of the fracture surfaces shows very little necking for all specimens. Spheroidal graphite cast iron does not have sufficient ductility to exhibit clear necking before failure. However, the formation of voids in spheroidal graphite cast iron occurs at a few percent strains for the large graphites [30]. The large graphites provide preferential sites for early void nucleation in the material. The failure path in ductile fracture is sensitive to the distribution of large second phase particles [31]. Therefore, almost all fractures occurred by dimpled rupture in the tensile specimens with various plastic constraint factors. However, a small amount of cleavage was observed in the central region of the fracture surfaces of R1 mm notched specimens, where the most severe triaxial stress state occurred. The development in stress triaxiality assists a microscopic fracture mechanism transition from microvoid coalescence to cleavage fracture.

Figure 10 shows the correlation between dimple area fraction and fracture strain. Almost all fracture surfaces were covered with dimples of various sizes, while, the fracture surfaces of R1 mm notched specimens with fracture strains of about 6% showed a mixture of dimpled rupture and small patches of cleavage fracture. However,

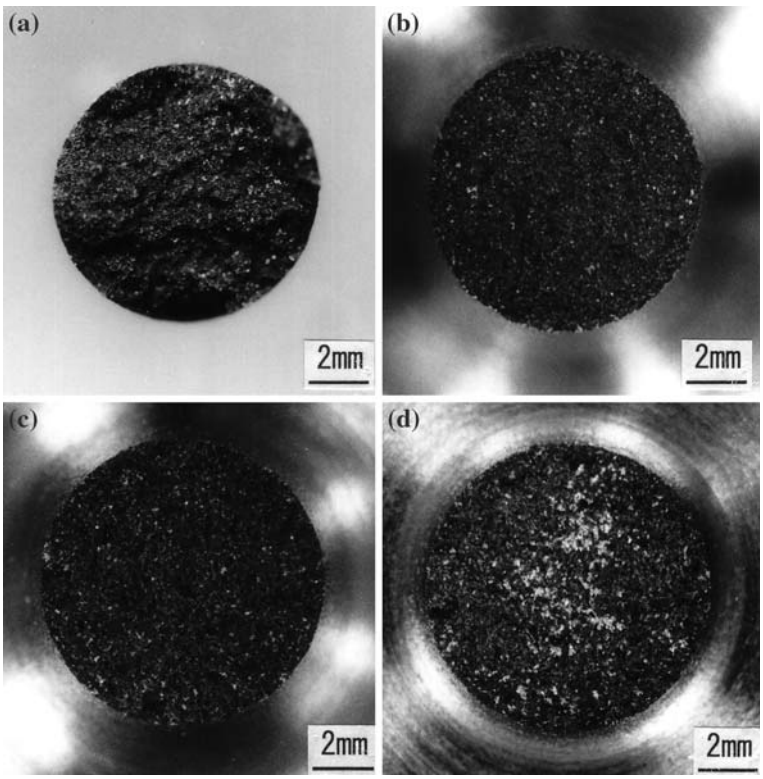

Fig. 9 Macroscopic fracture surfaces of unnotched and notched tensile specimens (**a**) Unnotched specimen (**b**) R6 mm notched specimen (**c**) R3 mm notched specimen (**d**) R1 mm notched specimen

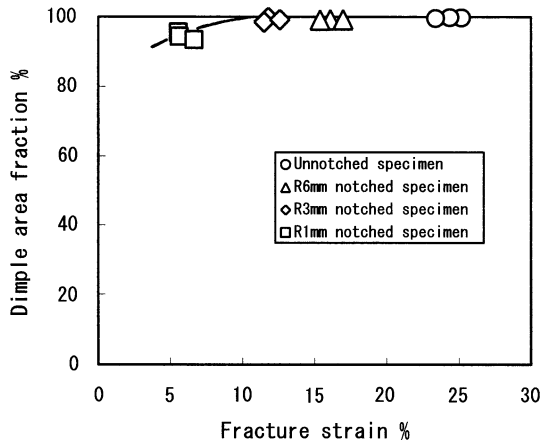

Fig. 10 Correlation between dimple area fraction and fracture strain

the area fraction covered by cleavage fracture is about 5% for R1 mm notched specimens. Thus, the dominant fracture mode is ductile fracture by dimpled rupture for all tensile specimens.

Extreme value probability plots of the maximum dimple sizes

The extreme value analyses of maximum dimple sizes were then performed on the fracture surfaces of all specimens. Figure 11 shows typical plots of the maximum dimple size

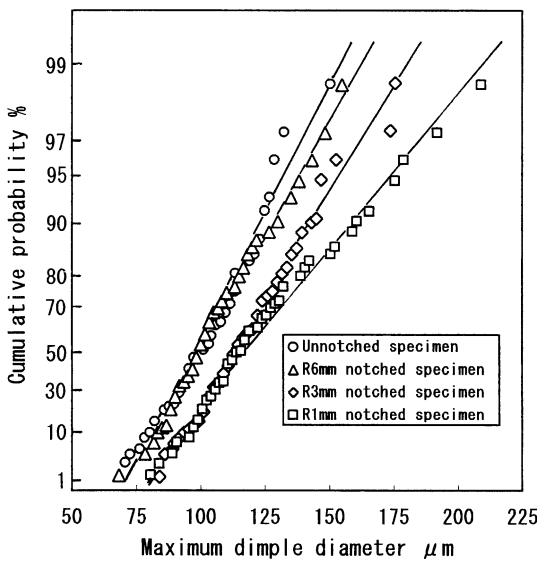

Fig. 11 Extreme value probability plots of maximum dimple sizes

data for four tensile specimens on an extreme value probability paper. The extreme value probability paper can be used conveniently for plotting the extreme values that follow the largest extreme value distribution, i.e., the so-called "Gumbel extreme value distribution". The distributions of the maximum dimple sizes were determined from a series of measurements of the maximum dimple sizes in 70 unit areas. The maximum dimple sizes were

arranged from smallest to largest, and plotted against cumulative probability. The best-fit lines to the plotted extreme values were drawn using the least-squares method.

Good straight lines were fitted for each set of maximum dimple size data for four tensile specimens with varying degrees of plastic constraint. This can be considered as good evidence that the distribution of the maximum dimple sizes could be expressed as largest extreme value distributions. In addition, the maximum dimple size distribution increased to a greater value with increasing plastic constraint due to an increase in notch acuity. On the other hand, the slope of the distribution decreased with increasing plastic constraint. This means that the variability of the maximum dimple size distribution becomes greater with increasing plastic constraint. Thus, the changes in the ductile fracture surface morphology of the four tensile specimens were well represented by the extreme value plots of the maximum dimple sizes.

Figure 12 shows typical micrographs of the fracture surfaces of the unnotched and R1 mm notched specimens. The scanning electron micrographs of the two specimens were prepared from equivalent views with a cumulative probability of about 90% in Fig. 11. Detached or broken graphites with a size of 10 μm to above 100 μm are visible in most dimples. The maximum dimple in each view is surrounded by a dotted line.

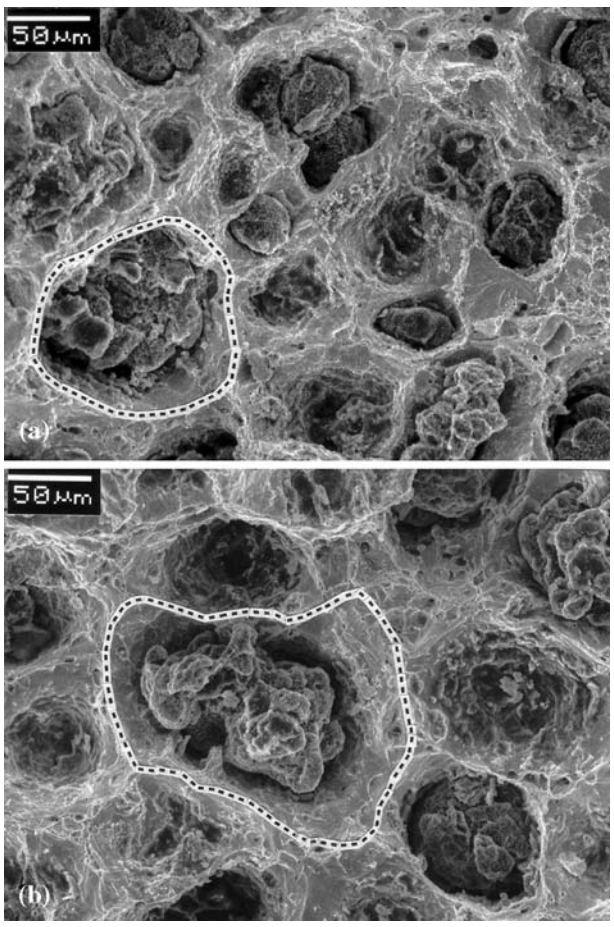

Fig. 12 Typical micrographs of fracture surfaces of unnotched and R1 mm notched specimens (**a**) Unnotched specimen (**b**) R1 mm notched specimen

The dimples separated by sharp-edged ridges have a wide range of sizes, although the boundaries are not clear for small dimples. However, a marked difference in the sizes of the maximum dimples is clearly demonstrated. In Fig. 12b, the maximum dimple for the R1 mm notched specimen shows a greater size under the influence of higher stress triaxiality compared with that for the unnotched specimen in Fig. 12a. Thus, the maximum dimple sizes in each view provide useful information about the magnitude of stress triaxiality. It should also be mentioned that the accuracy with which the size of the maximum dimple can be measured is higher than that for smaller dimples.

Dependence of location and scale parameters on plastic constraint factor

From Fig. 11, the distribution of the maximum dimple sizes can be expressed as a largest extreme value distribution. The cumulative distribution function of the largest extreme value distribution is given by Eq. 2

$$F(x) = \exp\,[\,-\exp\{\,-(x-\lambda)/\alpha\}\,] \qquad (2)$$

where λ and α are the location and scale parameters, respectively [18, 19]. Thus, the largest extreme value distribution is defined in terms of the two population parameters. The location parameter is a quantity to summarize the distribution, such as the mean, median, and mode, while, the scale parameter is a quantity related to the variability, such as the variance, standard deviation, and range of the distribution. For the largest extreme value distribution, the location parameter is the mode or highest point of the distribution, i.e., the maximum dimple size with most probable probability. It can be readily obtained as the maximum dimple size corresponding to a cumulative probability of $\exp^{-1} = 0.368$ on the extreme value probability paper. The scale parameter is $\sqrt{6}/\pi$ times the standard deviation of the distribution. It is given as the inverse ratio of the slope of the straight line fitted to the extreme value plots.

Figures 13 and 14 show the dependence of the location and scale parameters of the maximum dimple size distributions on the plastic constraint factor, respectively. Both parameters tend to increase with plastic constraint factor, although the correlations showed some scatter. The relations fitted to the experimental results were drawn using the least-squares method in Figs. 13 and 14. These results indicate that an increase in plastic constraint factor

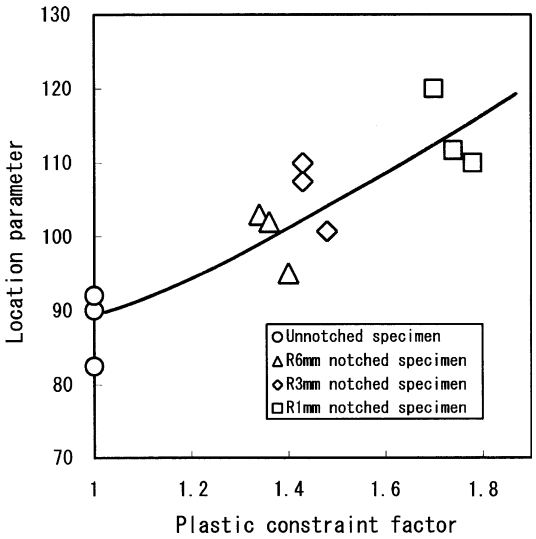

Fig. 13 Dependence of location parameter of maximum dimple size distribution on plastic constraint factor

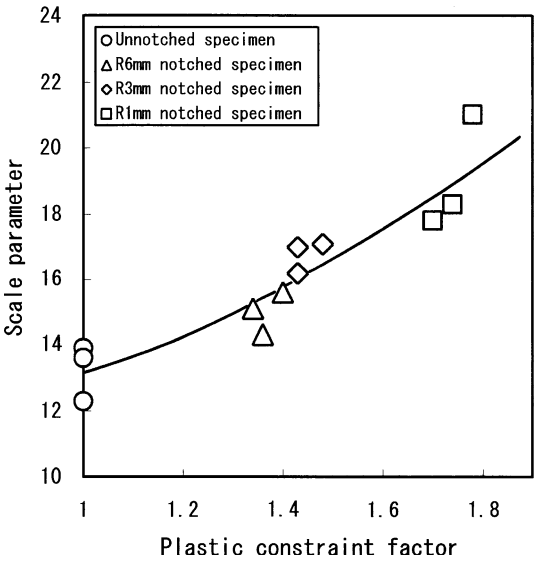

Fig. 14 Dependence of scale parameter of maximum dimple size distribution on plastic constraint factor

promotes more rapid growth and larger scattering in the distribution of the maximum dimple sizes.

On the other hand, Fig. 15 shows the Weibull distributions of the graphite sizes for three R1 mm notched specimens. The distributions of the graphite sizes ranging from about 10 to 130 μm were well represented as straight lines on the Weibull probability paper, indicating that the graphite size distribution could be described by the Weibull distribution. However, the distributions of the graphite sizes show a difference for the three specimens. A variation in the graphite size distribution can affect the distribution of dimple sizes. Therefore, the scatter in both

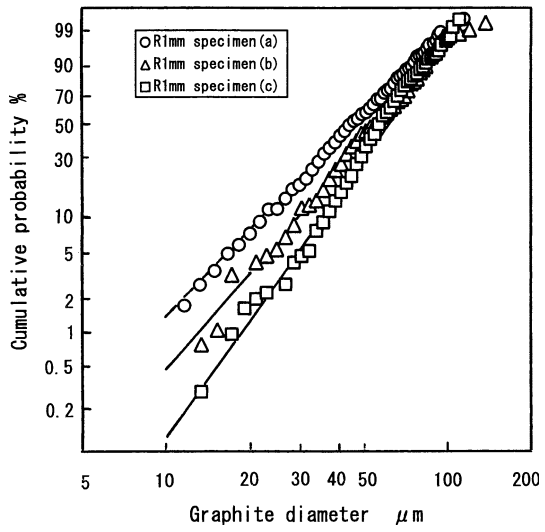

Fig. 15 Weibull distributions of graphite sizes

parameters of the maximum dimple size distributions in Figs. 13 and 14 could be attributed primarily to the statistical variation in the sizes of the graphites for each specimen.

Correlation of fracture strain and stress with location parameter

Figure 16 shows the correlation of fracture strain with location parameter, i.e., the maximum dimple size with most probable probability. Similarly, Fig. 17 demonstrates the variation of fracture stress with location parameter. The fracture strain decreased sharply with increasing location parameter, while, the fracture stress tends to increase with

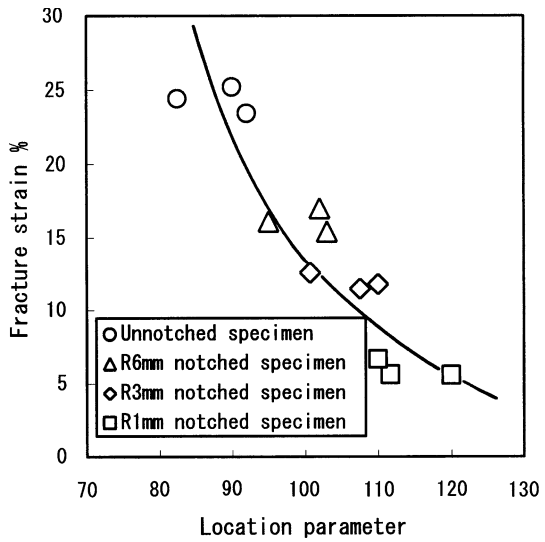

Fig. 16 Correlation of fracture strain with location parameter of maximum dimple size distribution

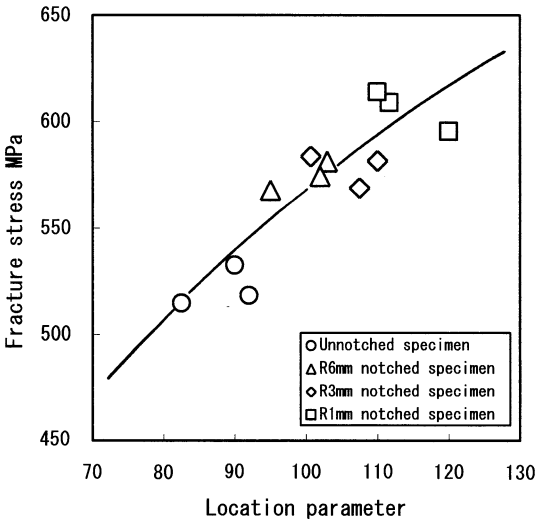

Fig. 17 Variation of fracture stress with location parameter of maximum dimple size distribution

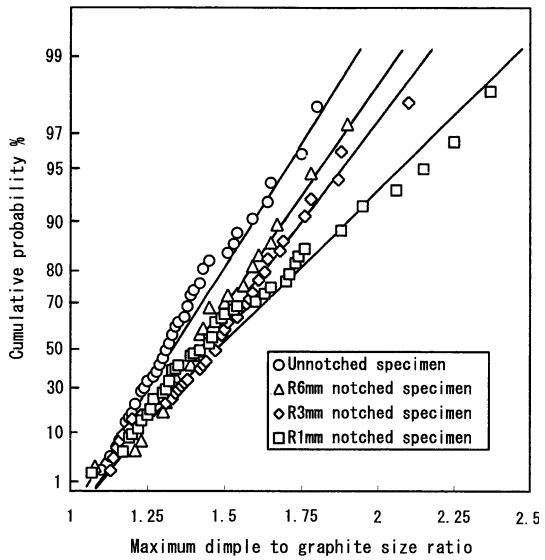

Fig. 18 Extreme value probability plots of lateral growth factors of maximum dimples

increasing location parameter. Thus, the fracture strain and stress were directly related to the location parameter of the maximum dimple size distribution. Once the location parameter is known from the extreme value plots of the maximum dimple sizes, the fracture behavior of the tensile specimen could be obtained approximately. It is valuable to be able to estimate the fracture behavior of the material based on a fractographic examination.

The fracture surface micro-roughness was used to obtain the fracture strain as a component of the fracture toughness [7, 8]. However, it is more convenient to measure the size of the dimple diameter on the ductile fracture surface. Therefore, extreme value analysis of the maximum dimple sizes could be used as an attractive method for a quantitative description of the ductile fracture surfaces associated with the fracture behavior of the material.

Extreme value probability plots of the lateral growth factors of maximum dimples

Figure 18 shows typical plots of the lateral growth factors of the maximum dimples for the four tensile specimens with various plastic constraint factors. The lateral growth factor was employed as an alternative parameter directly connected with stress triaxiality. The distributions of the lateral growth factors were well represented as good straight lines on the extreme value probability paper. The best-fit lines to the plotted extreme values were drawn using the least-squares method. Therefore, the distribution of the lateral growth factors of the maximum dimples could also be expressed as a largest extreme value distribution. It should also be noted that the distributions of the lateral growth factors are shifted to the right, and show a decrease in slope with increasing plastic constraint. This might be reasonably expected from the Rice and Tracey void growth equations [2], where the growth ratio of the spheroidal void is expressed as a function of stress triaxiality.

Figures 19 and 20 show the dependence of location and scale parameters of the distributions of the lateral growth factors on plastic constraint factor, respectively. The correlations also showed some scatter, however, both parameters show a clear tendency to increase with increasing plastic constraint factor. The relations fitted to the experimental results were drawn using the least-squares method in Figs. 19 and 20. Thus, an increase in plastic constraint factor also promotes a rapid growth and larger scattering in

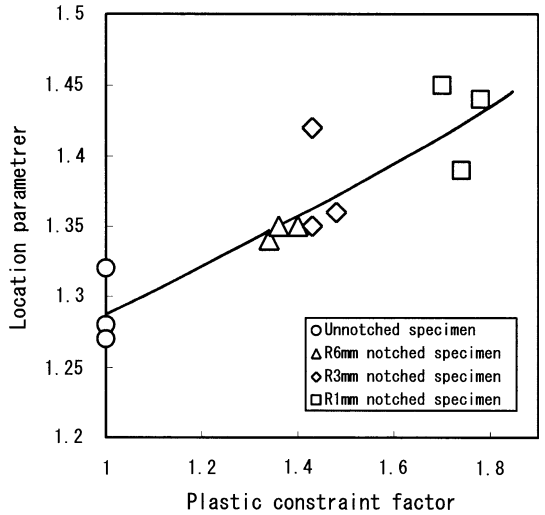

Fig. 19 Dependence of location parameter of lateral growth factor distribution on plastic constraint factor

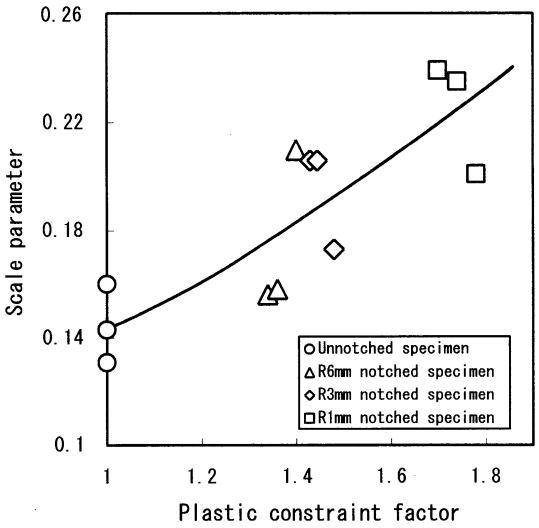

Fig. 20 Dependence of scale parameter of lateral growth factor distribution on plastic constraint factor

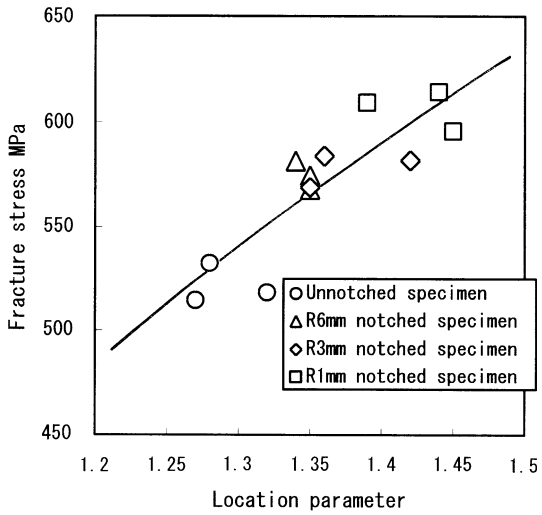

Fig. 22 Variation of fracture stress with location parameter of lateral growth factor distribution

the distribution of the lateral growth factors of the maximum dimples.

Figure 21 shows the correlation of fracture strain with location parameter of the distribution, while, Fig. 22 illustrates the variation of fracture stress with location parameter. The fracture strain decreased with increasing location parameter, whereas, the fracture stress shows a trend to increase with location parameter. The location parameter of the lateral growth factor distribution could be equally used as a good fractographic quantity associated with the fracture behavior of the tensile specimen.

A statistical variation is frequently observed for properties such as fatigue life and fracture strength of brittle materials. The stochastic approach was used to explain the

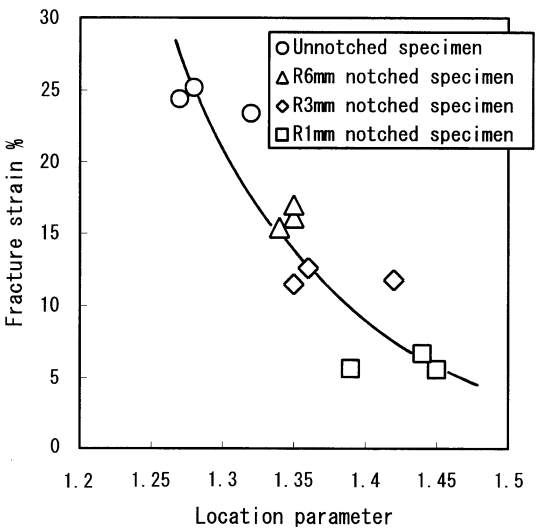

Fig. 21 Correlation of fracture strain with location parameter of lateral growth factor distribution

fatigue life and some other mechanical properties, which show much more scatter than the results of conventional mechanical tests. However, a similar situation arises in the quantitative description of the ductile fracture surfaces covered by differently sized dimples [32]. A wide spread in the sizes of dimples is an intrinsic nature of the ductile fracture surfaces, which has been a significant barrier for the quantitative description of ductile fracture surfaces. The sizes of dimples should be analyzed from a statistical point of view considering their wide scatter.

Therefore, extreme value analyses of both the maximum dimple sizes and lateral growth factors of maximum dimples were performed to describe the ductile fracture surface quantitatively connected to the fracture behavior of spheroidal graphite cast iron. The distributions of both the fractographic quantities were well expressed as largest extreme value distributions for all the tensile specimens with varying degrees of plastic constraint. In addition, the fracture strain and stress of the tensile specimen were directly related to the location parameter of the largest extreme value distribution, i.e., the maximum dimple size or lateral growth factor with most probable probability. As a result, the fracture behavior of the tensile specimen could be evaluated approximately once the location parameters of the distributions of both the quantities were known from fractographic examination. Moreover, extreme value analysis could be performed simply by measuring the extreme values in each view. Furthermore, the accuracy with which the size of the maximum dimple can be measured is higher than that for smaller dimples. Thus, extreme value analysis of both the fractographic quantities could be employed as an attractive method to obtain a quantitative description of the ductile fracture surfaces associated with the fracture behavior of spheroidal graphite cast iron.

Conclusions

Extreme value analysis of both the maximum dimple sizes and lateral growth factors of maximum dimples was performed correlated to the fracture behavior of spheroidal graphite cast iron. The main conclusions are as follows.

(1) The distributions of both the maximum dimple sizes and lateral growth factors of maximum dimples were well expressed as largest extreme value distributions for the tensile specimens with various plastic constraint factors.
(2) The location parameters of the distributions of both the fractographic quantities were directly related to the fracture strains and stresses of the tensile specimens. Therefore, the fracture behavior of the tensile specimen could be estimated approximately once the location parameter is known from fractographic examination.
(3) Extreme value analysis of the maximum dimple sizes and lateral growth factors could be employed as an attractive method to obtain a quantitative description of the ductile fracture surfaces associated with the fracture behavior of spheroidal graphite cast iron.

References

1. McClintock FA (1968) J Appl Mech 35:363
2. Rice JR, Tracey DM (1969) J Mech Phys Solids 17:201
3. Broek D (1973) Engng Fract Mech 5:55
4. Bray JW, Handerhan KJ, Garrison WM Jr., Thompson AW (1992) Metall Trans A 23A:485
5. Bray JW, Maloney JL, Raghavan KS, Garrison WM Jr. (1991) Metall Trans A 22A:2277
6. Thompson AW (1987) Metall Trans A 18A:1877
7. Thompson AW, Ashby MF (1984) Scripta Metall 18:127
8. Thompson AW (1985) TMS- AIME, Warrendale, PA 177
9. Stuwe HP (1980) Engng Frac Mech 13:231
10. Otsuka A, Miyata T, Nishimura S, Kimura M, Mabuchi M (1980) J Mater Sci Japan 29:717 (in Japanese)
11. Thompson AW (1983) Acta Metall 31:1517
12. Gumbel EJ (2004) Statistics of Extremes. Dover Pub., N.Y
13. Aziz PM (1956) Corrosion 12:495
14. Eldredge GG (1957) Corrosion 13:67
15. Hawn DE (1977) Mater Performance 16:29
16. Finley HF, Toncre AC (1964) Mater Protection 3:29
17. Ichikawa M, Takamatsu T, Matsumura T, Sawada T (1993) JSME Int J Ser A 36:121
18. Beretta S, Murakami Y (1998) Fatigue Fract Engng Mater Struct 21:1049
19. Beretta S, Ghidini A, Lombardo F (2005) Engng Fract Mech 72:195
20. Mackenzie AC, Hancock JW, Brown DK (1977) Engng Fract Mech 9:167
21. Hancock JW, Mackenzie AC (1976) J Mech Phys Solids 24:147
22. Thomson RD, Hancock JW (1984) Int J Fract 26:99
23. Orowan E (1948) Rep Prog Phys 12:185
24. Ritchie RO, Knott JF, Rice JR (1973) J Mech Phys Solids 21:395
25. Griffiths JR, Owen DRJ (1971) J Mech Phys Solids 19:419
26. Knott JF (1966) JISI 204:104
27. Oates G (1969) JISI 207:353
28. Bowen P, Knott JF (1984) Metal Sci 18:225
29. Tvergaard V, Needleman A (1984) Acta Metall 32:157
30. Harada S, Yano M, Endo T, Kawaguchi N (1988) Trans JSME A-54:925 (in Japanese)
31. Needleman A, Tvergaard V (1987) J Mech Phys Solids 35:151
32. Cox TB, Low JR Jr. (1974) Metall Trans 5:1457